Proceedings of the 9th U.S. National and 10th Canadian Conference on Earthquake Engineering
Compte Rendu de la 9ième Conférence Nationale Américaine et
10ième Conférence Canadienne de Génie Parasismique
July 25-29, 2010, Toronto, Ontario, Canada • Paper No 46

ESTIMATION OF CUMULATIVE ABSOLUTE VELOCITY (CAV) FROM A RECENTLY COMPILED STRONG GROUND-MOTION DATABASE FOR TURKEY

S. Akkar[1] and P. Gülkan[1]

ABSTRACT

The main context of the investigation that is reported herein is to develop an indigenous ground-motion prediction equation to estimate the Cumulative Absolute Velocity (CAV) parameter for nuclear installation safety. The recently compiled Turkish strong-motion database has used for this purpose. This report details the derivation of the predictive model as well as the ground-motion database used. The predictive model is compared with the CAV estimations of a similar model that is derived from a global database. Possible causes for differences are discussed.

Introduction

Cumulative absolute velocity was developed by the Electric Power Research Institute (EPRI, 1988) in response to insufficient representation of earthquake damage potential by the peak ground acceleration parameter. It has been demonstrated that CAV shows good correlation with macroseismic information and it takes into account the amplitudes and duration of the ground motion (Cabañas *et al*, 1997). These specific features suggest its consideration as one of the promising candidates for estimating ground-motion energy. In modern digital instruments with real-time processing capability, CAV can be calculated in real-time to provide immediate indication of earthquake damage potential. This property is particularly useful for the nuclear power community as well as many other industrial facilities as a rational criterion for earthquake shutdown.

This study presents a ground-motion prediction model for estimating CAV. The predictive model is derived from a recently compiled and processed Turkish strong-motion database that is confined to moment magnitude values between $4.0 \leq M_w \leq 7.6$ and source-to-site distances less than 200 km. The empirical relationship seems to make unbiased CAV estimations within the limits of the ground-motion dataset. A comparative evaluation of the predictive model is also presented at the end of the report after discussing the regression methodology and introducing the results for different cases. The predictive equation used for comparisons has been derived by Campbell and Bozorgnia (2008a). It uses a worldwide global dataset. Comparisons show that local and global predictive models can lead to different

[1] Earthquake Engineering Research Center, Department of Civil Engineering, Middle East Technical University 06531 Ankara, Turkey

estimates for a given ground-motion parameter depending on the particular features of the databases.

Cumulative Absolute Velocity

The generic definition of CAV for a given ground acceleration $a(t)$ is expressed in Eq. (1) (Kramer, 1996). It can be considered as the sum of the consecutive peak-to-valley distances in the velocity time history from a time interval between t_0 and $t_0 + D$. The commencement time (t_0) can be taken as $t = 0$ s. The ending time ($t_0 + D$), consequently, can be accepted as total record length. This way CAV can also be interpreted as the area under the absolute acceleration curve during the total record length. Therefore, CAV accounts for the contribution of both the amplitude and duration of the ground motion.

$$CAV = \int_{t_o}^{t_o + D} |a(t)|dt \tag{1}$$

Kennedy and Reed (EPRI, 1988) have been the proponents of CAV as one of the exceedance criteria for the definition of Operating Basis Earthquake (OBE) in nuclear power plants. That study defines the damage threshold level of nuclear power plants when the CAV value of a record is greater than 0.3 g-s and its 5%-damped response spectrum exceeds the OBE design spectrum level between 2 and 10 Hz . In 1991, the document EPRI TR-10082 (EPRI, 1991) modified the calculation of CAV. The threshold level of CAV for potential damage in nuclear power plants was reduced to 0.16 g-s. The standardized CAV calculation was re-defined as shown in Eq. (2) to remove the dependency of CAV on records of long duration containing low amplitude accelerations.

$$CAV = \sum_{i=1}^{n} \int_{t_i}^{t_i + 1} |a(t)|dt \tag{2}$$

In Eq. (2) $a(t)$ are acceleration values in a 1 s window, where at least one value exceeds a predetermined level of acceleration. This threshold level is typically accepted as 0.025g. Thus, the standard cumulative absolute velocity becomes the sum of n integrals of 1-s windows where the predetermined acceleration level is exceeded at least once. When the acceleration level is assumed as zero, the CAV will depend on the strong-motion duration definition. Figure 1 shows the variation of maximum horizontal component CAV (CAV_{Max}) with the moment magnitude that is determined from the strong-motion database used in this study. (Database details are given in the succeeding section). The consistent variation of CAV_{Max} with increasing magnitude emphasizes the sensitivity of this parameter to record duration as magnitude and strong-motion duration are in direct proportion. Though it is not shown in this report, a similar observation is also valid for the geometric mean variation for CAV.

Figure 2 shows the variation of CAV_{Max} with the maximum horizontal component of peak ground acceleration (PGA_{Max}) and peak ground velocity (PGV_{Max}) from the Turkish strong-motion database mentioned above. The CAV_{Max} values were computed with and without 0.025g threshold level to observe the effect of this parameter on the behavior of CAV in terms of other peak ground-motion parameters. The number of CAV data computed by implementing the threshold rule is smaller than the relaxed CAV data since many records failed to satisfy the threshold level. The threshold level seems to be dominant in CAV variation particularly for small amplitude cases. Inherently, differences in the variation of CAV computed with and without threshold become immaterial for large amplitude events. It should be noted that CAV

seems to draw a less dispersive behavior with PGV since both parameters predominantly feature the intermediate frequency components of ground motions.

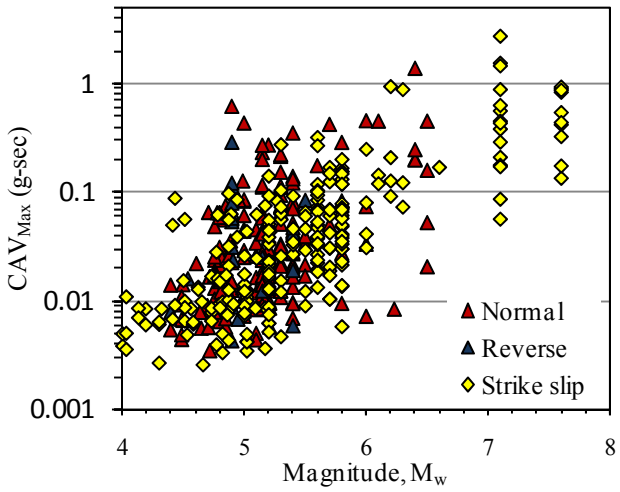

Figure 1. Maximum horizontal component CAV variation in terms of magnitude for different faulting styles. (0.025g threshold was not implemented in CAV calculations).

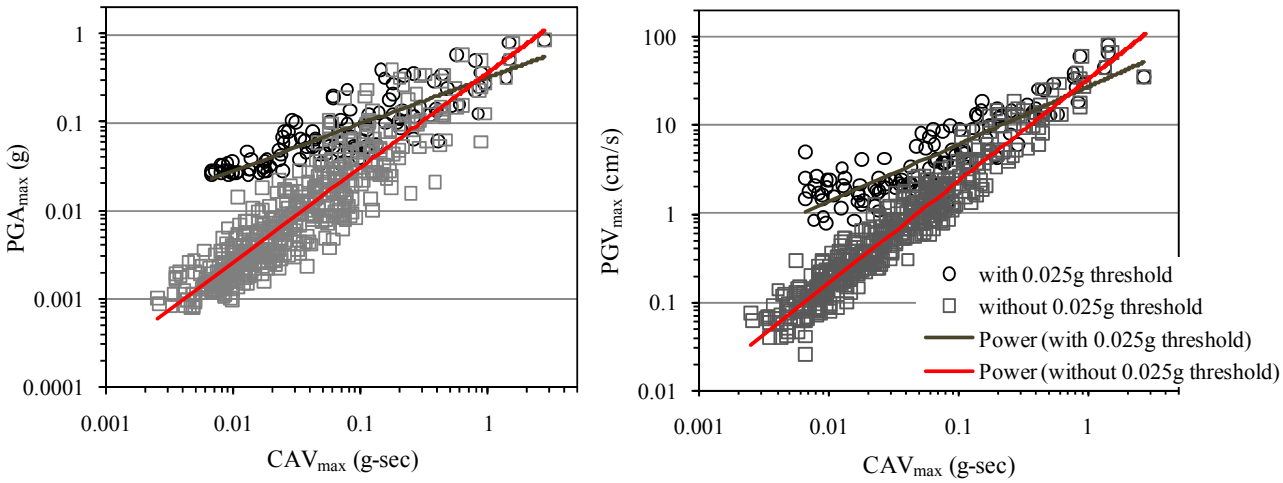

Figure 2. Relationships between CAV_{Max} and PGA_{Max} (left panel) as well as CAV_{Max} and PGV_{Max} (right panel) when 0.025g threshold level is implemented (black circles) and disregarded (gray squares) in CAV calculation. Straight lines are used for the qualitative description of dispersion level in CAV (with and without a given threshold) with the corresponding peak ground-motion parameter.

Strong-motion database

The Turkish strong-motion database (daphne.deprem.gov.tr) has been created as part of a project entitled "Compilation of Turkish strong ground-motion database in accordance with international standards" that was funded by the Scientific and Technological Research Council of Turkey under the Award No. 105G016. The faulting style was determined primarily from the plunges of P-, T- and B-axes using the criteria defined in Frolich and Apperson (1992). The

shear-wave velocity (V_s) vs. depth profile at each recording station was determined from the in-situ MASW surveys (Yılmaz *et al.*, 2008). The V_s profiles were used in strong-motion site classification that is based on the average shear-wave velocity of the upper 30 m soil layer ($V_{s,30}$). The moment magnitude vs. distance distributions of records in terms of faulting styles and site class are given in Figure 3. The majority of records are from normal and strike-slip faults and they are recorded on NEHRP C (360 m/s < $V_{s,30} \leq$ 760 m/s) and D (180 m/s < $V_{s,30} \leq$ 360 m/s) type sites. There are very few records from reverse and thrust faults and there is practically no rock site recording (NEHRP A and B site classes with $V_{s,30}$ > 760 m/s). The distance metrics used in this study are the closest distance to horizontal projection of rupture plane (R_{jb}) and the closest distance to rupture plane (R_{rup}) as these distance metrics are commonly used in predictive models. However, the database also contains source-to-site distance information for hypocental and epicentral distance. The magnitude interval of the database used in this study is between 4.0 $\leq M_w \leq$ 7.6. Although the data extends to distances up to 500 km, the majority is distributed within source-to-site distances less than 200 km. Details of the database are given in Akkar et al. (2010).

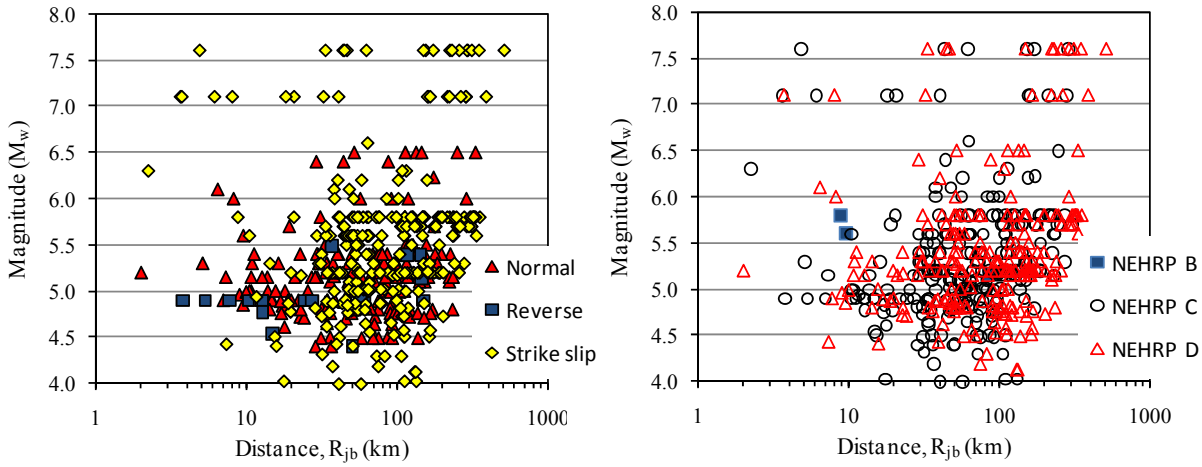

Figure 3. Magnitude (M_w) vs. distance (R_{jb}) scatter plots in terms of different style-of-faulting and site class. (Reverse faulting information contains both reverse and thrust fault data).

Regression Analyses

Random effects model (Abrahamson and Youngs, 1992) was used in the regression analysis. This model partitions the error into inter-event and intra-event terms to describe the variation between and within the earthquakes. The generic regression model has the following form

$$\log y_{ij} = f(M_w, r_{ij}, \theta) + \eta_i + \varepsilon_{ij} \qquad (3)$$

where y_{ij} is the ground-motion parameter, $f(M_w, r_{ij}, \theta)$ is the predictive model, M_w is the moment magnitude, r_{ij} is the source-to-site distance for the *jth* record from *ith* event and θ is the vector of other regression parameters. The regression model was derived for both R_{jb} and R_{rup} because these distance metrics can better describe the effect of wave propagation from source. The η_i represents inter-event variations and the ε_{ij} represents intra-event variations. The η_i and ε_{ij} are assumed to be independent, normally distributed variables with variances τ^2 and σ^2, respectively.

Figure 4 presents the distribution of events in terms of magnitude vs. distance scatters when CAV is computed with and without the 0.025g threshold level. The data distribution in Figure 4 indicates that implementation of 0.025g threshold level would result in insufficient resolution in terms of magnitude and distance. This deficient data would not describe a reliable variation of CAV in terms of magnitude, distance and other fundamental geophysical parameters (*i.e.* site class and faulting style). The results of preliminary regression analysis conducted by these two separate datasets support this observation. Therefore, predictive model results presented in this study are only valid for CAV estimations without a predefined threshold. As presented in Figure 4, the distance range for the predictive model is also limited to 200 km because there are very few events beyond this distance range (Figures 3 and 4). In essence, the regressions on CAV estimations are based on the data with $4.0 \leq M_w \leq 7.6$ and source-to-site distances less than 200 km.

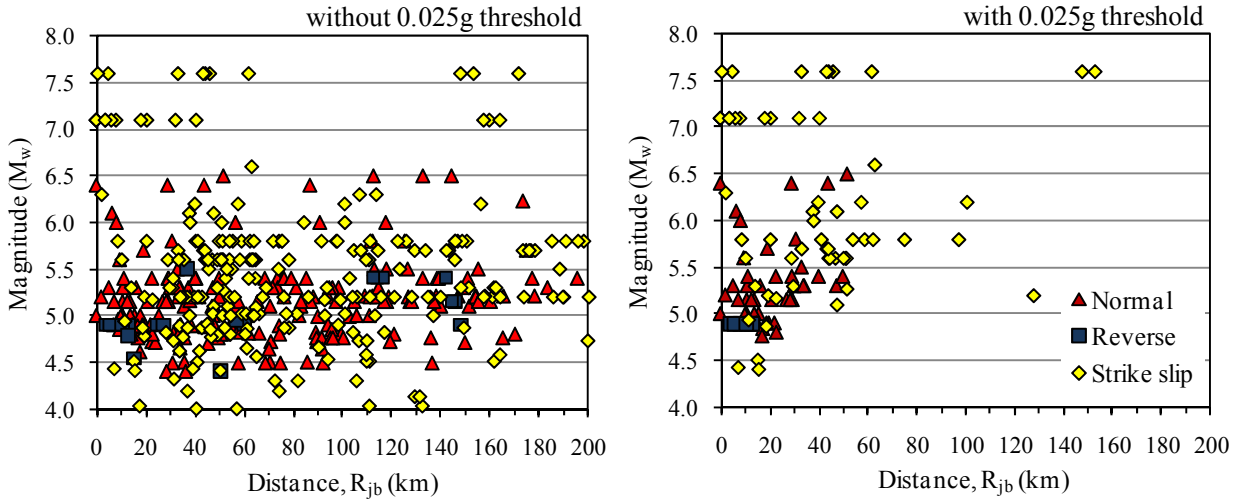

Figure 4. Magnitude vs. distance scatters in terms of different faulting styles. Left panel shows the data distribution when CAV is calculated without considering the threshold level (0.025g). Right panel depicts the same distribution when the aforementioned threshold level is considered. Reverse fault data considers both reverse and thrust fault events. The scatter distribution presented is approximately the same when the distance metric is changed from R_{jb} to R_{rup}.

The regression model used in this study is defined in Eq. (4). The model is quadratic in magnitude and accounts for magnitude-dependent geometric spreading. The anelastic attenuation term was dropped from the model because the pertaining regression coefficient attained an almost-zero positive number in the analysis. This suggests that the data distribution at large distances does not account for anelastic decay. The dummy arguments S_1 and S_2 are used to account for different site conditions. For NEHRP D site classes, S_1 and S_2 take values of 1 and 0, respectively. Both of these parameters are zero for rock sites (i.e. NEHRP B site class according to the database used) whereas $S_1 = 0$ and $S_2 = 1$ when site class is NEHRP C. In a similar manner, the dummy parameters S_N and S_R denote different faulting styles. The parameters S_N and S_R are 1 and 0, respectively for normal faulting events. S_N and S_R attain values of 0 and 1 for reverse events, respectively and $S_N = S_R = 0$ if the faulting is strike slip. The subscript *yy* in CAV either denotes the geometric mean (GM) or the maximum (Max) of horizontal components. The subscript *x* in *R* is used to distinguish R_{jb} and R_{rup}. The total

standard deviation (σ_{Tot}) of the regression model is composed of inter-event (τ) and intra-event (σ) components as described in the above paragraphs. No attempt was made to describe the variation of standard deviation in terms of explanatory variables used in the model. In other words, non-homogeneity, if it exists, in variance is ignored in the regression model. Table 2 lists the regression coefficients for the estimation of maximum and geometric mean components of CAV for R_{jb} and R_{rup}.

$$log_{10}(CAV)_{yy} = a_0 + a_1 M_w + a_2 M_w^2 + (a_3 + a_4 M_w)\, log_{10}\sqrt{a_5^2 + R_x^2} + a_6 S_1 + a_7 S_2 + a_8 S_N + a_9 S_R + \sigma_{Tot}; \qquad \sigma_{Tot} = \sqrt{\tau^2 + \sigma^2} \tag{4}$$

Table 2. Regression coefficients for CAV_{GM} and CAV_{Max} in terms of R_{jb} and R_{rup}

	a_0	a_1	a_2	a_3	a_4	a_5	a_6	a_7	a_8	a_9	σ	τ
CAV_{Max} in R_{jb}	-3.972	1.131	-0.074	-1.853	0.171	6.316	0.408	0.148	-0.033	-0.021	0.323	0.104
CAV_{Max} in R_{rup}	-3.756	1.139	-0.078	-2.022	0.190	6.548	0.398	0.128	-0.023	0.016	0.323	0.104
CAV_{GM} in R_{jb}	-4.076	1.141	-0.076	-1.851	0.173	6.228	0.440	0.187	-0.026	-0.013	0.318	0.102
CAV_{GM} in R_{rup}	-3.845	1.146	-0.079	-2.024	0.193	6.534	0.428	0.164	-0.016	0.023	0.318	0.102

Figure 5 shows the variation of CAV_{Max} estimations for different magnitude, site class and faulting styles, respectively. This figure illustrate that CAV estimations are consistent with the variations in magnitude, site class and distance. It should be noted that the predictive model can recognize the site class influence on CAV estimations although the database is quite non-uniform in terms of site class distribution (few rock site events as discussed in the previous section). This could be attributed to the powerful regression methodology implemented in this study. The magnitude-dependent decay results in a more gradual decrease in CAV at larger distances with increasing magnitudes. The magnitude-dependent gradual decrease of ground motions at large distances has also been recognized by the recent predictive models.

The influence of faulting style seems to be limited for CAV estimations as there are no significant differences between the CAV estimations from different fault types. The non-uniform distribution of database in terms of faulting style might be one reason for the indifferences in faulting-style dependent CAV behavior. One can also hypothesize that faulting style is not a prominent seismological parameter for ground-motion parameters that are dominated by intermediate frequency ground-motion components. This issue is discussed in detail by Bommer et al. (2003). The discussions presented here also apply to CAV_{GM} that is not shown for space limitations.

Figures 6 display the residual scatters for CAV_{GM} estimations. The left and right panels show the residual scatters as a function of magnitude and distance, respectively. The solid straight lines are least square fits to test whether the residuals have trends with the changes in magnitude and distance. Significant trends in the straight lines would point to biased estimations of the predictive model in terms of magnitude and distance. It can be observed that the variation of residuals is quite random with respect to magnitude and distance. In almost all cases, the solid straight lines follow the zero line ensuring once again that the estimations by Eq. (4) are unbiased for the dataset used in this study. This is also confirmed by calculating the F-statistics

of the slope of each straight line at 5% significance level. The F-statistics have shown that the slopes are not significantly different than zero at 95% confidence level.

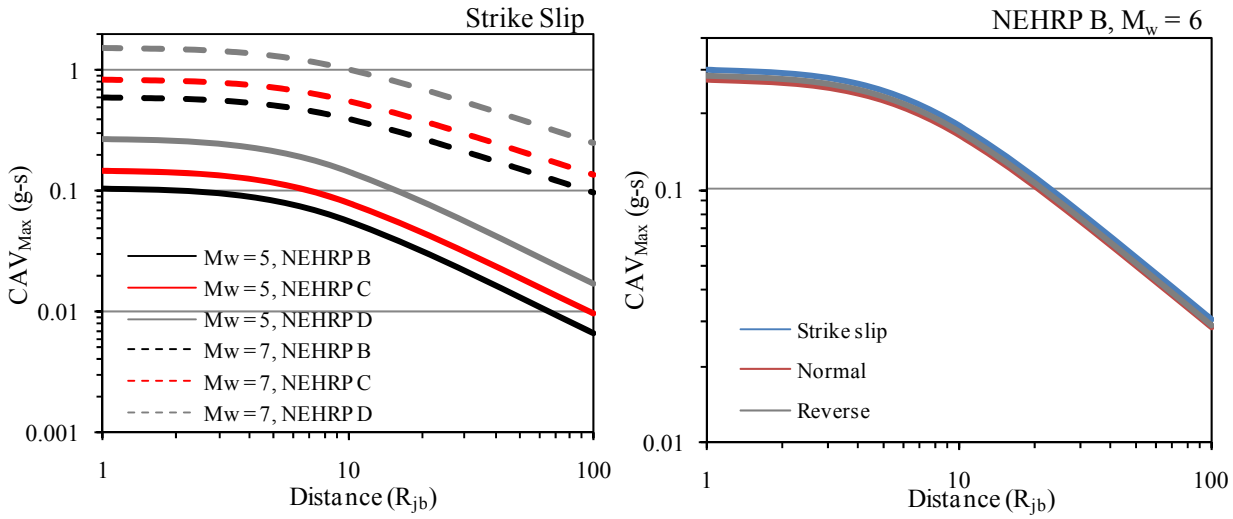

Figure 5. CAV_{max} estimations (left panel) of Eq. (4) at different site classes (NEHRP B to D) and magnitude levels (M_w = 5 and 7) for R_{jb}. The right panel describes the influence of different faulting styles on CAV_{max} estimations for a scenario event with M_w = 6 and NEHRP B site class.

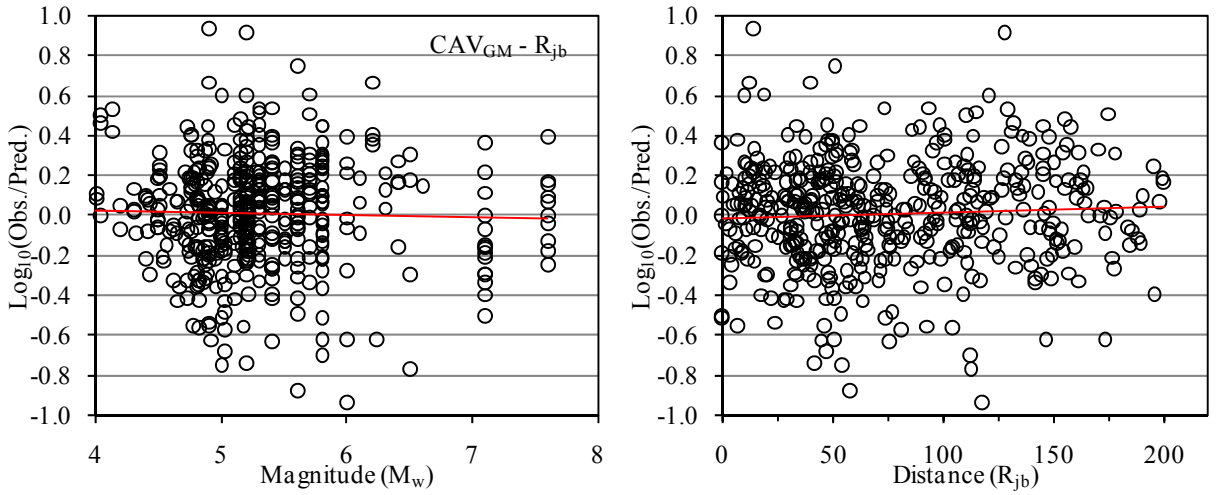

Figure 6. Residual scatters in terms of magnitude (left panel) and distance (right panel) for CAV_{Max} estimations when distance metric is R_{jb} in the regression model.

The regression model used in this study disregards nonlinear soil effects that can be particularly influential in the estimation of soft site CAV values. This possible deficit was investigated by conventional residual analysis as well by plotting the residuals against the estimated CAV values for NEHRP D class recordings. The results are shown in Figure 7 for CAV_{Max}. The least square straight line fits that are superimposed on each plot indicate a consistent conservative estimation of the predictive model as CAV attains larger values. However, the F-statistics revealed that the variations in straight lines are insignificant as their

slopes can be accepted as 0 at the 5% risk level. Thus, disregarding the soil nonlinearity effects does not result in substantially safer CAV estimations for the ground-motion dataset used in this study.

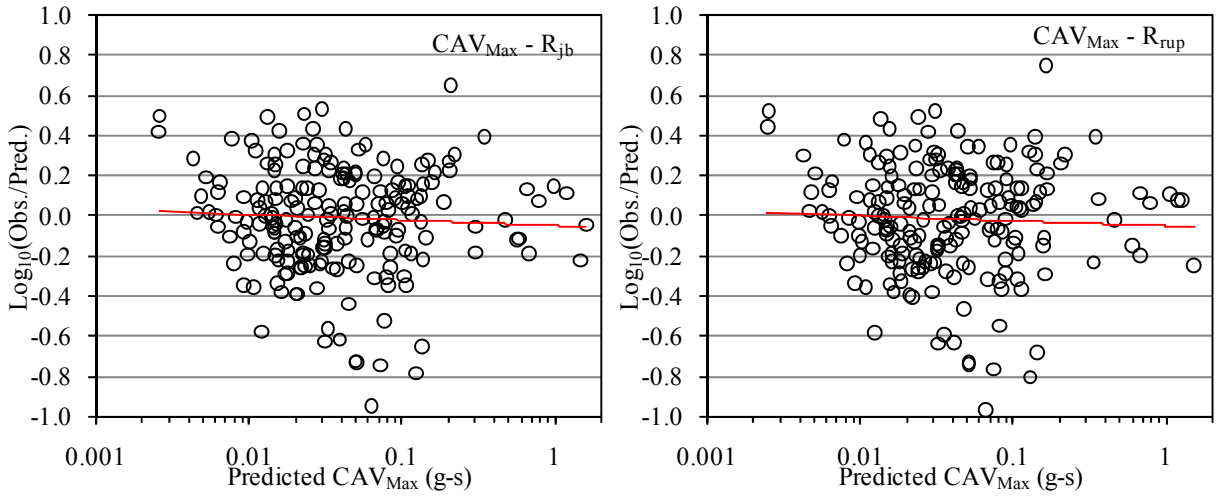

Figure 7. Residual scatters of NEHRP D class records against the estimated CAV values for the maximum horizontal components in terms of R_{jb} (left panel) and R_{rup} (right panel).

Comparisons with Campbell and Bozorgnia predictive model

Campbell and Bozorgnia (2008a) have derived a predictive model for the estimation of CAV_{Max}. The functional form of the predictive equation as well as the ground-motion dataset used by Campbell and Bozorgnia (2008a) are the same as those used for the NGA project (Campbell and Bozorgnia, 2008b). This empirical relationship (abbreviated as CB in the text) uses continuous $V_{s,30}$ values for defining site effects. It accounts for the soil nonlinearity by using the median peak acceleration on a rock outcrop and constrain the nonlinear site response terms using the results of 1D analytical site response model of Walling et al. (2008). Soil/sediment depth effect (basin effect) is also considered in this model for modeling site amplification through the estimation of depths where V_s = 2.5 km/s (Z2.5). CB model describes the basin effect bearing on the 3D simulations of Day et al. (2008) with additional empirical adjustments at shallow soil/sediment depths. Additionally, CB accounts for the rupture-depth effect in reverse earthquakes by defining the depth-to-top of rupture (Z_{TOR}) parameter for depths greater than 1 km. The rationale behind this term is the relatively stronger shaking of buried ruptures with respect to the surface ruptures at the same distance.

Figure 8 shows the comparisons of CAV_{max} estimates computed from the predictive model of this study and Campbell and Bozorgnia. The comparisons are done for M_w = 5 and M_w = 7 strike-slip scenarios on NEHRP site classes C and B. Since local soil conditions are taken into account by continuous $V_{s,30}$ in CB, NEHRP C and D site classes are described by $V_{s,30}$ = 460 m/s and 285 m/s, respectively in this model . These are the geometric mean $V_{s,30}$ values of corresponding strong-motion sites in the dataset. The comparisons are done in terms of R_{rup} as CB is originally based on this distance metric. The plots in Figure 8 indicate that CB model tends to overestimate CAV_{max} with respect to the predictive model of this study as the site becomes softer. The correlation between the two models is very well for NEHRP C type site

class (i.e. $V_{s,30}$ = 460 m/s). In general, CB estimations for NEHRP D sites are twice larger than the CAV_{max} estimations of this study. The increased discrepancy in NEHRP D site CAV_{max} estimations can be attributed to the differences in data distribution of soft site recordings. Owing to its worldwide character, the database used in CB model may cover a more complete variation of CAV_{max} in terms of geophysical and geotechnical features for NEHRP D type recordings. The differences in the functional terms used in describing the site effects can also play a role on the divergent CAV_{max} estimations between the two empirical equations. CB model considers continuous $V_{s,30}$ and uses a sophisticated model to describe the site influence on ground motions that is discussed in the previous paragraph. In this study, the site effects are handled in a simpler manner by classifying the site effects into three broad groups. Therefore, the variation of $V_{s,30}$ within a site category is ignored. Detailed analyses are required on the two databases and functional forms to address the significance of above points to reveal the observed differences in CAV_{max} estimations. This is out of the scope of this study, and might constitute the focus of a follow-up investigation.

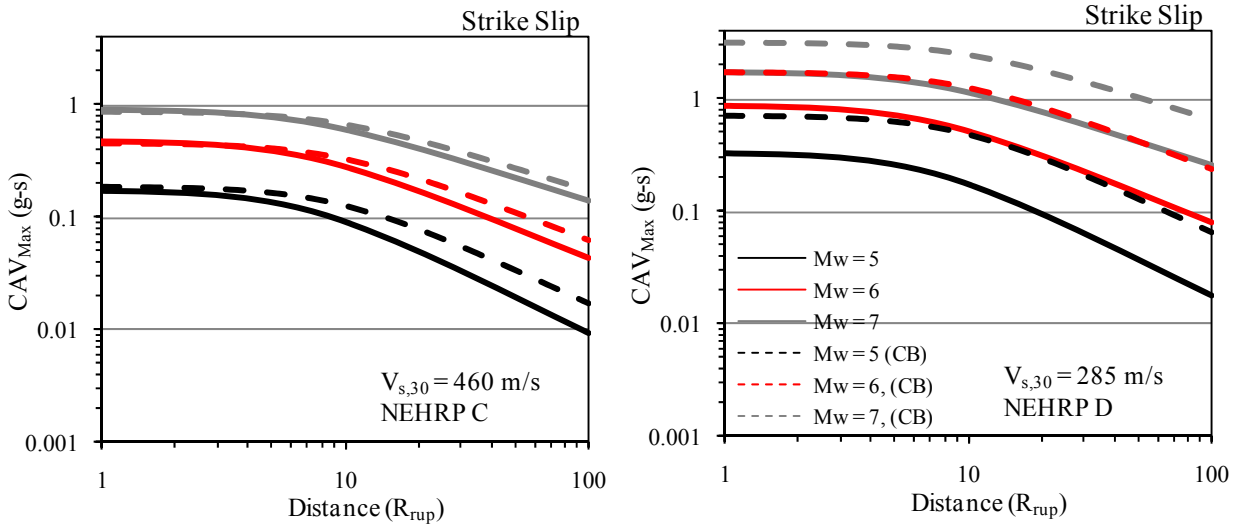

Figure 8. Comparison of CAV_{Max} that are estimated from the predictive equations of this study and Campbell and Bozorgnia (2008a). The comparisons are done for strike slip events with M_w = 5, 6 and 7. The left and right panels compare the CAV_{Max} estimations for NEHRP site classes C and D, respectively.

Summary and Conclusions

This report describes a predictive model for estimating CAV_{max} and CAV_{GM} form recently compiled Turkish strong-motion database. Based on the extent of the database, the predictive model is valid for $4.0 \leq M_w \leq 7.6$ and source-to-site distances (either R_{jb} or R_{rup}) less than 200 km. The predictive model can account for the variations in site class (NEHRP B, C and D) and faulting style (Normal, strike slip and reverse) while estimating the maximum and geometric mean CAV amplitudes. The residual analysis indicated that the predictive model yields unbiased estimations confined to the geophysical and geotechnical limits imposed by the database. The predictive model presented in this study is compared with a similar purpose empirical relationship derived by Campbell and Bozorgnia (2008a) that uses a global ground-motion dataset. The comparisons reveal a fairly good match for NEHRP C site CAV estimations. However, there is considerable discrepancy between the two models at softer sites

(NEHRP D) that can stem from the differences in databases (local vs. global) or functional forms. Table 2 is the summary of the findings reported in this document.

Acknowledgements

This research is funded by the Scientific and Technical Research Council of Turkey with award no. 105G016. The contributions of Earthquake Research Department of the General Directorate of Disaster Affairs during this project are acknowledged by the authors. International Atomic Energy Agency also provided partial funding under the Contract No. BC:5381 170 3509 J4030261 to run CAV analysis. The authors express their sincere gratitude to this suport.

References

Abrahamson N. A. and R. R. Youngs (1992). A stable algorithm for regression analyses using the random effects model, *Bulletin of the Seismological Society of America*, Vol. 82, 505-510.

Akkar S., Z. Çağnan, E. Yenier, Ö. Erdoğan and A. Sandıkkaya (2010). The recently compiled Turkish strong-motion database: preliminary investigation for seismological parameters, *Journal of Seismology*, Vol. 14.

Bommer J.J., J. Douglas and F.O. Strasser (2003). Style-of-faulting in ground-motion prediction equations, *Bulletin of Earthquake Engineering*, Vol. 1, 171-203.

Building Seismic Safety Council (BSSC) (2003). *The 2003 NEHRP recommended provisions for new buildings and other structures. Part 1: Provisions (FEMA 450)*, Federal Emergency Management Agency, Washington, DC.

Cabañas, L., B. Benito and M. Herraiz (1997). An approach to the measurement of the potential structural damage of earthquake ground motions, *Earthquake Engineering and Structural Dynamics*, Vol. 26, 79-92.

Campbell, K. and Y. Bozorgnia, (2008a). Preliminary relationships between Cumulative Absolute Velocity (CAV) and JMA instrumental intensity (I_{JMA}) and preliminary attenuation relationships for CAV and I_{JMA}, IAEA CS on Alternative Ground Motion Scaling in Attenuation Relationships: *Progress and Planning in the USA, Progress Report #1*, May 16, 2008.

Campbell, K. W. and Bozorgnia, Y., (2008b). NGA ground motion model for the geometric mean horizontal component of PGA, PGV, PGD and 5% damped linear elastic response spectra for periods ranging from 0.01 to 10 s, *Earthquake Spectra*, Vol. 24, 139-171.

Day, S. M., R. Graves, J. Bielak, D. Dreger, S. Larsen, K. B. Olsen, A. Pitarka, and L. Ramirez-Guzman (2008). Model for basin effects on long-period response spectra in Southern California, *Earthquake Spectra*, Vol. 24, 257-277.

EPRI, (1991). Standardization of the cumulative absolute velocity, *EPRI TR-100082 (Tier 1)*, Electric Power Research Institute, Palo Alto CA.

EPRI, (1988). A criterion for determining exceedance of the operating basis earthquake, *EPRI NP-5930*, Electric Power Research Institute, Palo Alto CA.

Frohlich, C. and K. D. Apperson (1992). Earthquake focal mechanisms, moment tensors, and the consistency of seismic activity near plate boundaries, *Tectonics*, Vol. 11, 279–296.

Kramer, S. L., (1996). *Geotechnical Earthquake Engineering*, Prentice Hall Inc., Upper Saddle River, New Jersey.

Walling, M., W. Silva, and N. Abrahamson (2008). Nonlinear site amplification factors for constraining the NGA models, *Earthquake Spectra*, Vol. 24, 243-255.

Yılmaz, Ö., E. Savaşkan, S.B. Bakır, M.T. Yılmaz, M. Eser, S. Akkar, B. Tüzel, Y. İravul, Ö. Özmen, Z. Denizlioğlu, A. Alkan and M. Gürbüz (2008). Shallow seismic and geotechnical site surveys at the Turkish national grid for strong-motion seismograph stations, *Proceedings of 14th World Conference on Earthquake Engineering*, Beijing, China, Paper No. 03-03-0013.